RAA 2018 Vol. **18** No. **4**, 42(10pp) doi: 10.1088/1674–4527/18/4/42

http://www.raa-journal.org *http://iopscience.iop.org/raa*

***R**esearch in*
***A**stronomy and*
***A**strophysics*

Method of composing two-dimensional scanned spectra observed by the New Vacuum Solar Telescope

Yun-Fang Cai[1,2], Zhi Xu[1] , Yu-Chao Chen[1,2], Jun Xu[1], Zheng-Gang Li[1], Yu Fu[1] and Kai-Fan Ji[1]

[1] Yunnan Observatories, Chinese Academy of Sciences, Kunming 650011, China; *xuzhi@ynao.ac.cn*
[2] University of Chinese Academy of Sciences, Beijing 100049, China

Received 2017 November 9; accepted 2018 January 8

Abstract In this paper we illustrate the technique used by the New Vacuum Solar Telescope (NVST) to increase the spatial resolution of two-dimensional (2D) solar spectroscopy observations involving two dimensions of space and one of wavelength. Without an image stabilizer at the NVST, large scale wobble motion is present during the spatial scanning, whose instantaneous amplitude can reach 1.3″ due to the Earth's atmosphere and the precision of the telescope guiding system, and seriously decreases the spatial resolution of 2D spatial maps composed with scanned spectra. We make the following effort to resolve this problem: the imaging system (e.g., the TiO-band) is used to record and detect the displacement vectors of solar image motion during the raster scan, in both the slit and scanning directions. The spectral data (e.g., the Hα line) which are originally obtained in time sequence are corrected and re-arranged in space according to those displacement vectors. Raster scans are carried out in several active regions with different seeing conditions (two rasters are illustrated in this paper). Given a certain spatial sampling and temporal resolution, the spatial resolution of the composed 2D map could be close to that of the slit-jaw image. The resulting quality after correction is quantitatively evaluated with two methods. A physical quantity, such as the line-of-sight velocities in multiple layers of the solar atmosphere, is also inferred from the re-arranged spectrum, demonstrating the advantage of this technique.

Key words: instrumentation: spectrographs — Sun: sunspots — techniques: imaging spectroscopy — techniques: image processing

1 INTRODUCTION

Spectroscopy in two spatial dimensions (two dimensions of space and one of wavelength) is widely used by a large number of quantitative measurements of atmospheric structures in the field of solar physics that are only retrieved from high resolution spectral observations, such as pressure, density, temperature, velocity, etc. (Fang & Huang 1995). Classical methods to acquire such two-dimensional (2D) spectroscopy mainly include: narrow-band filtergrams, multi-channel subtractive double pass (MSDP, Mein 1977) spectrographs and spatial scanning of slit spectrographs. Each approach has its own specific advantages and drawbacks. With a narrow-band filtergram, for example, using a Fabry-Perot Interferometer (FPI, Bonaccini & Stauffer 1990), monochromatic images are taken at successive wavelengths across a spectral line. Spectral line synthesis at each spatial position needs to be obtained within a certain time interval by this wavelength scan. The spectral resolution is on the order of 30 mÅ (e.g., the report by Puschmann et al. 2012). By contrast, the MSDP mode can provide monochromatic images at different wavelengths simultaneously. But its shortcoming is that the observed field-of-view (FOV) is inversely proportional to the spectral resolution, which means only a moderate spectral resolution can be achieved for a reasonable FOV. For instance, the MSDP installed in Meudon Solar Tower can provide images at nine wavelength points simultaneously with an FOV of 71″ (perpendicular to the slit direction) × 465″

(slit direction) and the wavelength distance is about 0.3 Å (Mein et al. 2009). Spatial scanning is the method usually utilized together with a slit spectrograph. It enables one to use all the features of the spectrograph, such as high spectral (better than about 20 mÅ) and spatial resolution, wide wavelength range and simultaneous observations of multiple spectral lines. One can control the telescope movement or equip a field scanner in front of the spectrograph to do spatial scanning, i.e., to move the solar image through the entrance slit continuously and rapidly. As is known, a faster scanning speed should be better for a given solar active region since the dynamic structure of the Sun continuously evolves with time. Compared with telescope drift, it is easy to use a field scanner to move the solar image fast and control the scanning speed according to the exposure time or other operations (e.g., the polarimetric modulation at each slit position for the spectro-polarimetry observation).

Usually for ground-based observations, it is not so easy to move the solar image rigidly in the right direction that is perpendicular to the entrance slit. The influence of both the Earth's atmosphere and the precision of the telescope guiding system might cause the image to wobble in both the slit and scanning directions. A 2D map directly composed by the spectral data, which are sequentially obtained with time during scanning, could have a very low spatial resolution (Keller et al. 1990). Solar structures even show discontinuities or zig-zag morphologies in this case. So in addition to the long time consumption mentioned above, another important aspect involved in spatial scanning is how to guarantee the entrance slit is located at a correct position during scanning. Some efforts have been made and techniques developed to try and resolve this issue. For instance, Johanneson et al. (1992) carried out the simultaneous acquisition of spectral data and slit-jaw images. A series of slit-jaw images was used to monitor the image motion during scanning, allowing the spectrum to be re-mapped spatially during the data processing. Soon after, a solar correlation tracker was developed (Ballesteros et al. 1996), which could be used as an image stabilizer and an accurate positioning device to achieve 2D high spatial resolution spectra in real time (Collados et al. 1996). Nowadays, adaptive optics (AO) systems have generally been utilized by ground-based telescopes to resolve the problems of image motion and distortion induced by the Earth's atmosphere. Such facilities include the German Vacuum Tower Telescope (Mikurda et al. 2006), Gregory-Coudé Telescope (Sütterlin & Wiehr 2000), New Solar Telescope (NST) (Cao et al. 2010), etc.

In this paper, we present a technique used by the New Vacuum Solar Telescope (NVST) (Liu et al. 2014) in order to increase its spatial resolution when acquiring 2D spectra. This is similar to the method suggested by Johanneson et al. (1992), but the specific details are different. The amplitude of the wobble motion is much larger in our case since there is currently no image stabilizer or AO system operating at NVST. We will elucidate the data processing procedure step by step in the following sections.

The paper is organized as follows: Section 2 introduces the characteristics of the instrument and observational setups. Section 3 describes our technique in detail. In Section 4 we evaluate the composed image quality resulting from this technique. The conclusions and discussion are given in Section 5.

2 INSTRUMENTATIONS AND OBSERVATIONS

NVST is a vacuum solar telescope with a 985 mm clear aperture located at the Fuxian Solar Observatory, administered by Yunnan Observatories (Liu et al. 2014). Two instruments are currently operational at the facility. One is the high-resolution multi-channel imaging system (Xu et al. 2014; Xiang et al. 2016), including two broad-band interference filter channels (TiO-band and G-band) and three narrow-band Lyot filter channels (Hα, Ca II 3933 Å and He I 10830 Å). The other is the multi-wavelength spectrograph in visible lines, working at Hα, Ca II 8542 Å and Fe I 5324 Å lines (more information can be found in Wang et al. 2013). The imaging system and the spectrograph have identical foci and are arranged to be perpendicular to each other as illustrated in Figure 1. Incoming light is redirected into these two instruments with different percentages using a beam splitter. We employ different kinds of beam splitters to optimize the observation wavelengths for either simultaneous or independent operation of these two instruments. In addition, the slit position can be precisely determined in the FOV of the imaging system by an optical calibration technique (Fu et al. 2016). An introduction to this calibration process is beyond the scope of this paper, but we demonstrate the result in Figure 2. In this way the imaging system can serve as a slit-jaw recorder for spectroscopy, despite the slit being invisible. A field scanner is installed in front of both instruments and comprises

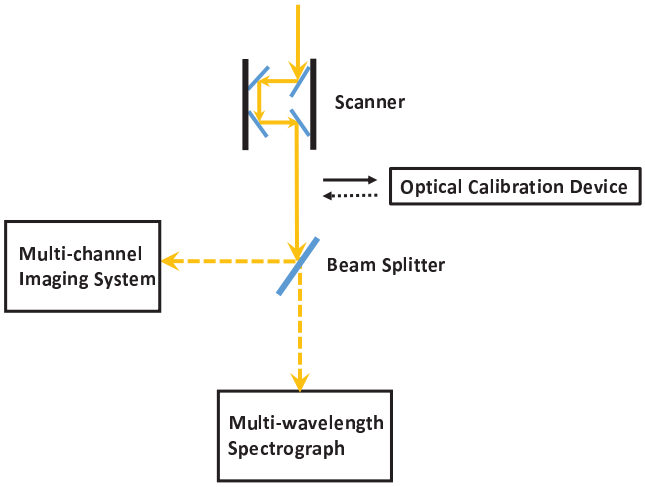

Fig. 1 Schematic of the optical layout of the NVST instruments (Not to scale).

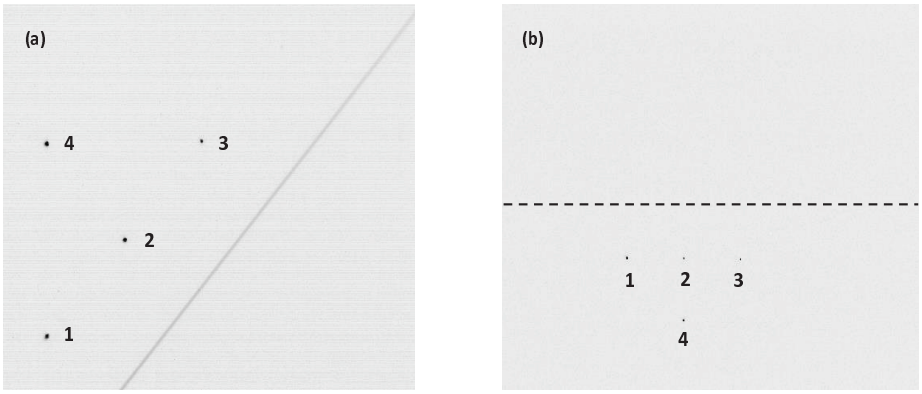

Fig. 2 Determination of the slit position in the FOV of the TiO image. (a) An image taken by a optical calibration device. Both the entrance slit of the spectrograph and a four-pin-hole diaphragm sitting at the focal plane of the imaging system are clearly seen. (b) An image of the four-pin-hole diaphragm taken in the TiO channel. The position of the entrance slit can be derived from the relative displacement shown in panel (a) and indicated by a *dashed line*.

two pairs of K mirrors as shown in Figure 1. One pair of K mirrors moves along the optical path to produce the solar image motion in the direction perpendicular to the slit (refer to Yang et al. 2016 for more details).

In the present work we select a beam splitter which permits 90% of photons to transmit into the spectrograph and 10% of photons to enter the imaging system in order to obtain broad-band filter images in the TiO channel and high signal-to-noise (SNR) spectra of the Hα line (SNR $>$ 100), simultaneously. TiO images are used to detect the solar image motion, including both scanning and wobble motions. However, at present the TiO images are not synchronously recorded with Hα spectral data. When serving as a slit-jaw recorder, the camera for the TiO channel operates with 4×4 binning. The recording rate is then about 15 frames per second with an acquisition time of 60 ms. This is comparable to the value of Hα spectral observations, which are taken typically with a 60 ms exposure time and 40 ms readout time, resulting in an acquisition time of about 100 ms and a recording rate of about 10 frames per second. Last but not least, the spectral data are taken synchronously with positioning of the field scanner.

The FOV in the TiO channel (slit-jaw) is about 133″ × 112″ with pixel sampling of about 0.21″. For spectral observations, the FOV is about 129″ in the slit direction. We usually raster about 110–120 steps with a step size identical to the slit width (0.45″), which corresponds to about 50″– 55″ on the solar surface. If we totally take five frames at each scanning position (this parameter is adjustable), it takes approximately 60 seconds to accomplish such a 110-step raster.

We acquired 2D spectral observations of several active regions. In the following, we illustrate our technique to increase the spatial resolution based on two raster observations of the active regions NOAA 12661 (2017 June 7) and NOAA 12671 (2017 August 22). The latter has better seeing conditions than the former.

3 METHODS

3.1 Pre-processing

Pre-processing of the slit-jaw (TiO) images includes flat-field and dark correction. Unlike Johanneson et al. (1992), we do not need to remove a vertical slit from the slit-jaw images. Precise data pre-reduction of the spectra has been done by Cai et al. (2017), which is adapted from the method proposed by Wang et al. (2013), but this process is specifically applicable for the raster observations. The data reduction comprises flat-field correction, dark subtraction and distortion correction of spectral lines. In addition, both the wavelength calibration and continuum intensity modification are carefully applied to all the spectral data in order to ensure accuracy of the quantities (e.g., the line-of-sight (LOS) velocity) retrieved from the spectral data. In other words, each specific spectra line has an identical pixel position in all the data to facilitate the following process of 2D map composition. One frame of the reduced spectral data and a quasi-simultaneous TiO image are shown in Figure 3.

3.2 Calculating the Displacement Vectors

As a first step, TiO images are used to measure the solar image motion during the raster in both the slit and scanning directions. As mentioned above, we usually raster an area of about 60″ in the scanning direction, which can be fully covered by the FOV of the TiO image. In contrast to Johanneson et al. (1992), we need not reconstruct a reference slit-jaw image, which is supposed to have a larger FOV to completely cover the observation target throughout the raster. In our case, we choose the middle frame of the TiO images to be the reference frame and calculate the displacement vector of other frames with respect to it using a cross-correction technique. For the observations in our study, sunspot features facilitate this tracking method. The image motion during one scan is shown in Figure 4. It is found that, in addition to the linear motion in the scanning direction represented by a linear fitting, there exists a wobble motion in both the slit and scanning directions. The amplitude of this wobble can reach up to 1.3″, which is almost three times the step size (0.45″).

Next, we determine the solar image motion at the time when the spectrogram was observed. We are reminded that the acquisition speed of the TiO slit-jaw image is comparable to that of the Hα spectrogram although they are not synchronous. We assume that variation of the image motion changes linearly with time between two nearby TiO samples, then we apply a linear interpolation to the displacement vectors detected from the TiO slit-jaw images at the time when the spectrum was taken.

Figure 5 shows the displacement vectors of the TiO slit-jaw images and the interpolated vectors of the Hα spectral data spanning about 3 seconds.

3.3 Correction and Re-arrangement of Spectral Data

The motion along the slit direction is easily corrected by shifting the spectral data with the corresponding displacement vectors in the slit direction. However, the motion in the scanning direction needs to be corrected by re-arranging the spectral data according to the displacement vectors in the scanning direction. Due to the wobble motion accompanying the raster scan, the solar surface cannot be evenly scanned by the slit, so that the spatial sampling in the scanning direction is not equal to the scan step size. Supposing we initially set the scan step size equal to the slit width (0.45″) and considering spectra whose displacement vectors are within the range $n \times 0.45'' - (n+1) \times 0.45''$ as the ones taken at the n-th scanning position, we find that the number of frames at each scanning position is quite different from the initial number (i.e., five frames).

Figure 6 illustrates one example. It is a 110-step raster scan over the active region NOAA 12661 taken on 2017 June 7 with step size equal to 0.45″ and temporal resolution of 60 s. It is seen that there are different numbers of frames corresponding to the spectral data

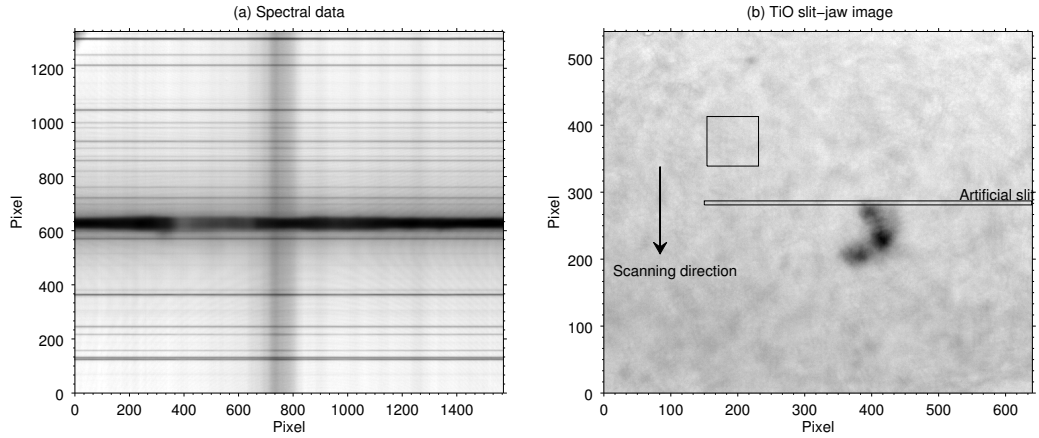

Fig. 3 (a) One spectrogram in the Hα channel after the precise pre-process. (b) One TiO slit-jaw image taken quasi-simultaneously with the spectrum. An *elongated rectangle* marks the position of the entrance slit. The *arrow* indicates the scanning direction. A *box* outlines the area in which the intensity is integrated and used to evaluate the intensity variation with time.

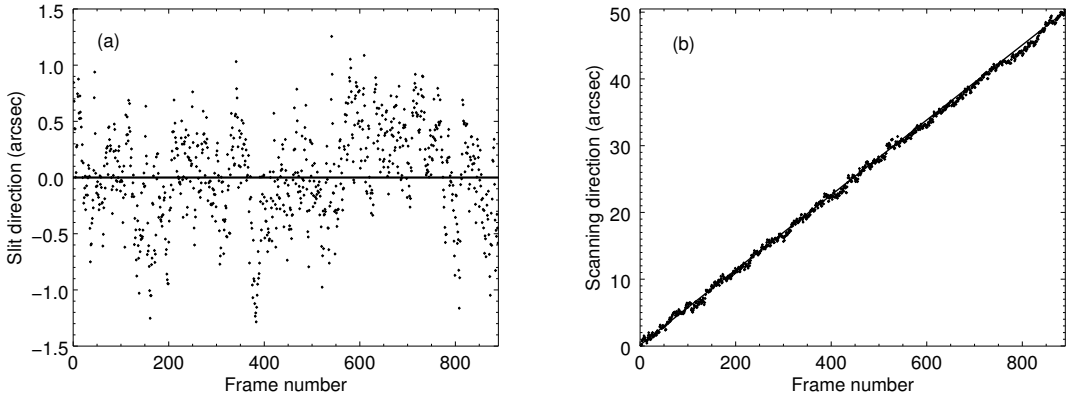

Fig. 4 Displacement vectors inferred from the TiO slit-jaw images during one scan in both the slit (a) and scanning (b) directions. A *solid line* in each panel represents a least-squares linear fit.

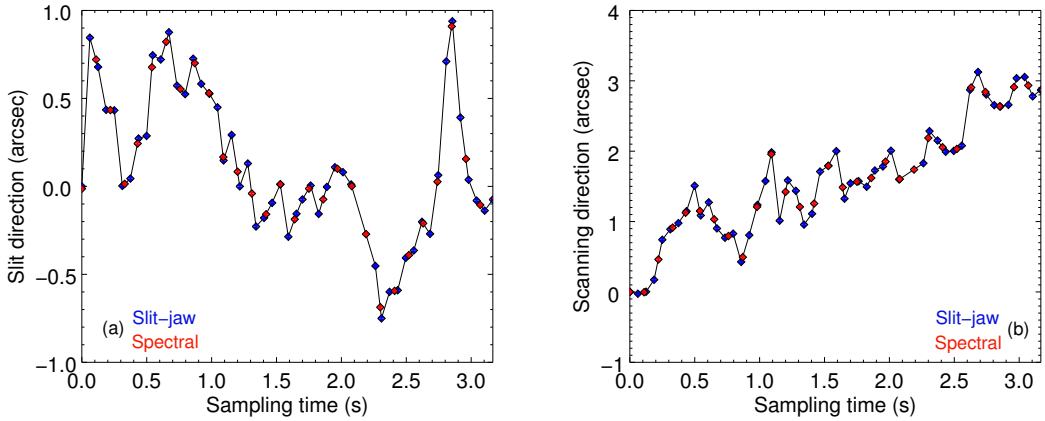

Fig. 5 Displacement vectors in both the slit (a) and scanning (b) directions spanning about 3 seconds. Imaging motions at the times when the Hα spectral data (the TiO slit-jaw image) are taken are represented by *red* (*blue*) *rhombi*.

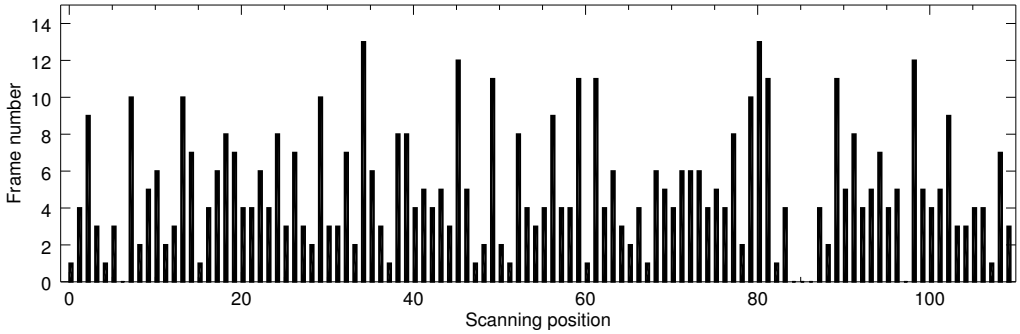

Fig. 6 Number of frames at each scanned position after rearrangement.

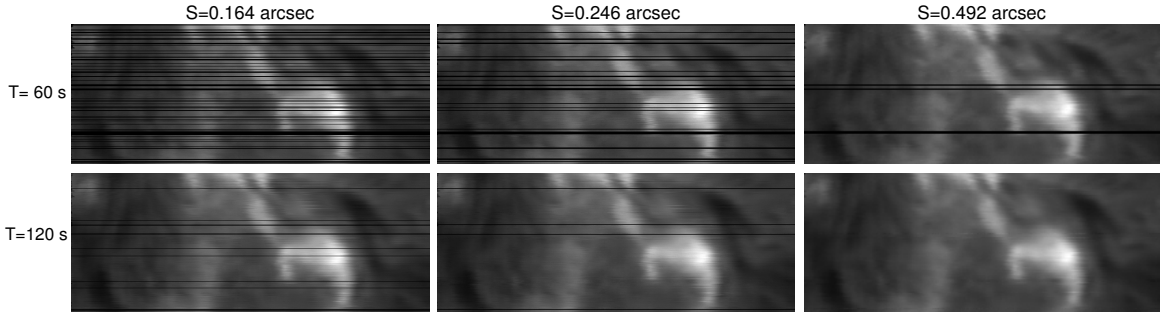

Fig. 7 Two-dimensional intensity map of the active region NOAA 12661, composed at the Hα line center with the different spatial samplings and temporal resolutions.

re-arranged into one scanning position. The maximum number of frames is 13 while the minimum is 0, which indicates that some areas are scanned multiple times but some are not scanned at all.

3.4 Composing into a Two-dimensional Map

At last, we combine all the spectra into 2D maps. We implement different strategies for the composition in the two situations mentioned above, i.e., the multiple-frame and 0-frame cases at each scanning position.

Case 1: When there are multiple frames present at one scanning position, we take the averaged frame of the multiples with the assumption that all of them basically correspond to the same position on the solar surface within certain spatial and temporal resolutions. Actually, we also apply the frame-selection methods with different criteria, such as selecting the spectrum that is taken when the quasi-simultaneous TiO slit-jaw image has the strongest image contrast or identifying the spectrum which shows the deepest specific line depth. However we do not find any distinct improvement in the quality of the composed image, and we therefore use the averaged frame in practice.

Case 2: If there are no frames at a scanning position, we usually apply cubic-interpolation to the neighboring values when the 2D composed image is generated. However, when such a 0-frame case occurs at many scan steps, we need to consider a new spatial sampling and temporal resolution to re-arrange the spectral data in space, instead of relying on a fixed step size. As shown in Figure 7 (from left to right respectively), we consider different spatial samplings of $0.164''$, $0.246''$ and $0.492''$ with 60 s temporal resolution, to re-arrange the sequentially observed spectral data into the correct positions. When the spatial sampling is set as small as $0.164''$, which is about two times the pixel sampling along the slit used to acquire the spectral data ($0.082''$/pixel), it is found that several scanning positions show 0-frame cases, which are displayed by black lines in the composed monochromatic intensity map. However when we decrease the spatial sampling to a value of $0.492''$, the number of black lines becomes much fewer.

Alternatively, we can increase the number of initial frame acquisitions at each scan step or combine several successive scans into one. Of course, this inevitably decreases the temporal resolution of the raster scan. Also, as shown in Figure 7, we compose a 2D intensity map using the spectral data taken in two successive scans (i.e., in the bottom row). This case is equal to taking *one* dense scan over the 50″ FOV, but the time consumption (i.e., the time evolution) is correspondingly extended by about 120 s.

In short, both the spatial sampling and temporal resolution have to be reasonably taken into account when re-arranging the spectra in order to eventually compose a 2D map that meets the differing needs of various scientific studies.

4 RESULTS AND EVALUATION

We compare 2D composed intensity maps before and after solar motion correction in Figure 8. Two different observations are exhibited. Figure 8(a)–(f) shows a 110-step raster over the active region NOAA 12661 on 2017 June 7, while Figure 8(g)–(j) shows a 100-step raster over NOAA 12671 on 2017 August 22. The left column displays results which are directly composed by spectra taken sequentially, and the right column features the ones composed by spectra re-arranged in the scanning direction and corrected in the slit direction. The spatial sampling is considered to be the same for both data sets (i.e., equal to the initial scan step size of 0.45″). It is clearly seen that some solar structures in the original map have many more burrs than those in the map after the motion correction, particularly in the regions pointed out by the arrows, such as sunspots with strong intensity contrast in the photosphere (e.g., Fig. 8(a), (b), (g) and (h)) and a filament located at the adjacent quiet region (e.g., Fig. 8(c) and (d)). We also find that although the seeing in the second data is much better than that in the first, the burrs are still clearly present around the sunspots. This means that most of these burrs are caused by malposition and drift of the slit position during scanning.

The above burrs can result in intensity fluctuation and even structure deformation in 2D maps, therefore we use two methods to quantitatively evaluate the composed images. Firstly we select a sub-region in which sunspots or bright structures are present. Then we calculate the second-order finite differences in this region using every three neighboring pixels. The *rms* of the second-order finite difference reflects the intensity fluctuation. For example, in the first observation we focus on a bright plage seen in the monochromatic image of the Hα line center (Fig. 8(e) and (f)). The *rms* is calculated to be about 0.021 based on the original 2D map and 0.015 based on the corrected image. In the second observation which has a better seeing condition, we focus on a sunspot area visible in the monochromatic image at continuum (Fig. 8(g) and (h)). The *rms* is about 0.020 before the motion correction and becomes 0.016 after it. Both results demonstrate that almost 1/4 of the intensity fluctuation is caused by burrs, which is eliminated after the motion correction. Secondly, we compare the similarity between the 2D intensity image composed at continuum (see Fig. 8(a-b) and (g-h)) and the TiO slit-jaw images. This comparison is in terms of the Structural Similarity Index Measurement (SSIM). The TiO slit-jaw images need to be firstly resized to the same spatial resolution as the composed maps. Specifically, for the first observation, the SSIM between the TiO slit-jaw image and Figure 8(a) is about 0.85. After the motion correction (e.g., Fig. 8(b)), the SSIM is about 0.91. For the second observation, the SSIM increases from about 0.90 to 0.94 after the motion correction. In brief, quantitative evaluations resulting from the two methods show the quality of the raster images is improved after motion correction. It is also found that given a certain spatial sampling and temporal resolution, the spatial resolution of the composed 2D map could be close to that of the slit-jaw image.

Besides the measured quantities like line intensity, we can also obtain a 2D map of inferred quantities like the LOS velocity. The LOS velocity is derived using the center-of-gravity method from a specific line profile. Moreover, the 32 Å-wavelength range in the Hα band allows us to observe photospheric and chromospheric lines simultaneously. In addition, telluric lines can also be used as wavelength references to calculate the absolute LOS velocity. In Figure 9, we display the LOS velocities of two active regions in the photosphere in panels (a) and (c). These images were retrieved from the photospheric Fe I (6574.2 Å) line. Besides the granular pattern of velocity, large-scale Evershed flows around sunspots are clearly present along the penumbral filaments. It is revealed that the speed varies from around 1 km s^{-1} at the border between the umbra and the penumbra to a maximum of 1.8 km s^{-1} in the middle of the penumbra and falls off to zero at the outer edge of the penumbra. This spatial distribution is in agreement with a previous ob-

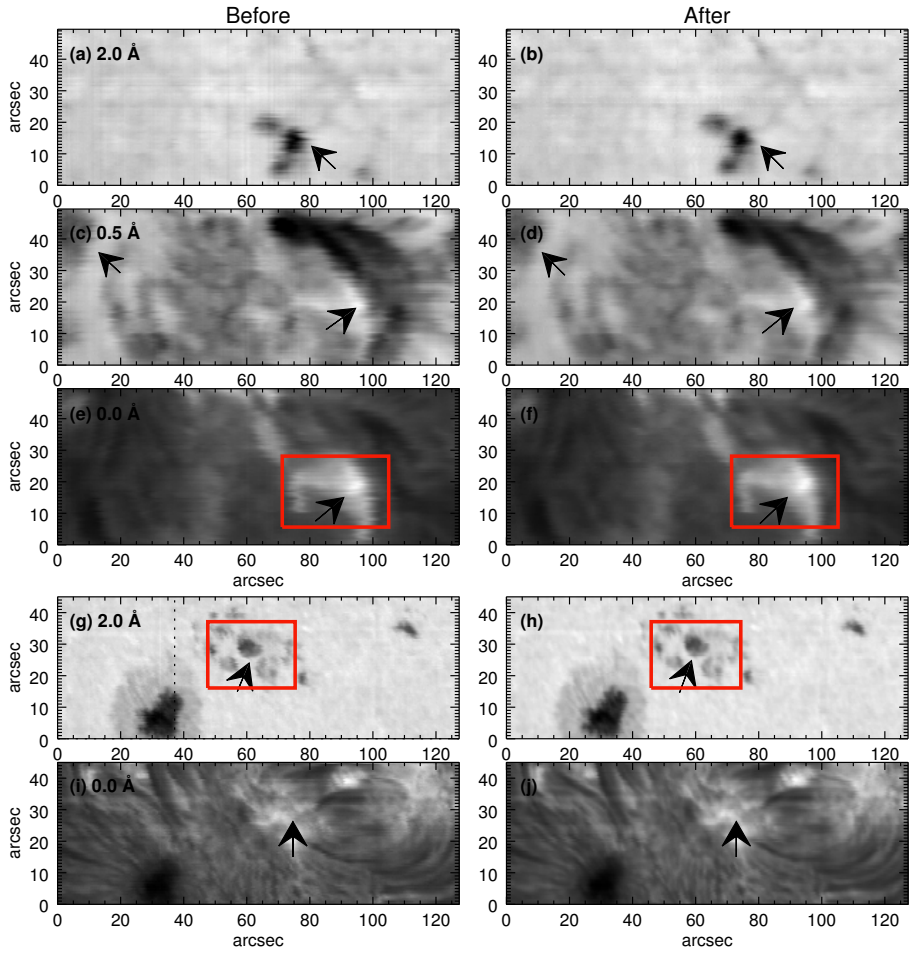

Fig. 8 Two-dimensional composed intensity map at different wavelengths. (a–f) A 110-step raster over the active region NOAA 12661. (g–j) A 100-step raster over the active region NOAA 12671. Two-dimensional maps are composed and shown at different wavelengths around the Hα line as the notes indicate (2.0 Å, 0.5 Å and 0 Å.). *Red rectangles* outline the sub-regions in which second-order finite differences are calculated and compared.

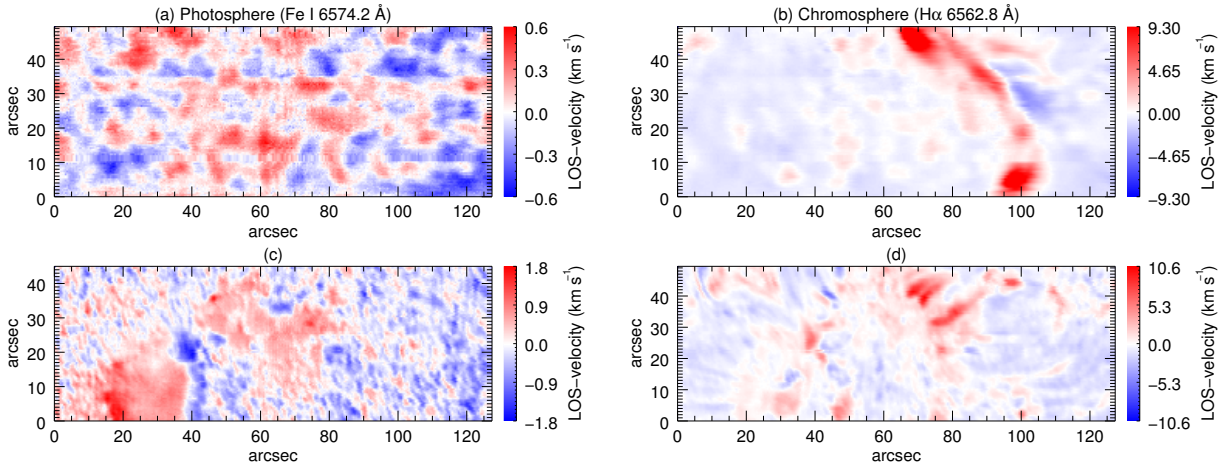

Fig. 9 Two-dimensional Doppler velocity maps retrieved from the scanned spectra over the active regions NOAA 12661 (a-b) and NOAA 12671(c-d).

servation (Rimmele & Marino 2006). Panels (b) and (d) are LOS velocities in the chromosphere inferred from the Hα line. Although the Evershed flow around sunspot is not very distinct here, our other observational data clearly show a reversal flow present in the chromosphere (Xu et al. 2010). In addition, large scale velocities are found around the filament structure, while fast downflows are detected at the footprints of the arch filament system.

5 CONCLUSIONS AND DISCUSSION

Our system allows us to employ multi-channel high resolution imaging with a multi-wavelength spectrograph co-temporally, co-spatially and co-focally at the NVST. The slit position can be precisely determined in the FOV of the imaging system, which makes it possible to use the imaging system as a slit-jaw recorder to monitor the solar image motion during the scanning, even though there is no visible slit in its FOV.

Taking advantage of this convenience, we detect the spectra displacement vectors of the solar image motion during the spatial scanning from broad-band imaging observations (e.g., the TiO-band). The displacement vectors include both the scanning and wobble motions. Without any image stabilizer, the random motion of the solar image under study could instantaneously reach up to 1.3 arcsec or more, which is almost three times larger than the spatial sampling (typically equal to the slit width, 0.45″) and severely decrease the spatial resolution of the 2D spectroscopy observations.

As a next step, these displacement values need to be linearly interpolated to get the values when the spectral data (e.g., the Hα) are quasi-simultaneously taken. At present, the slit-jaw images and spectral data are not synchronously acquired, but the acquisition rates are comparable. After that, the series of spectral data originally taken in time sequence are corrected (in the slit direction) and re-arranged (in the scanning direction) in space. Two techniques are used to evaluate the resulting quality of the newly composed 2D maps. The spatial resolution is fairly improved and close to the one of the slit-jaw images.

However, a small amount of burrs still exist in the corrected raster 2D maps. It is obvious at the edge of solar structures which are expected to be smooth. The reason could be that the acquisition speeds of spectral data and slit-jaw images are not strictly synchronized. The interpolated displacement vectors of the spectral data might be different from the real case. Synchronous observations need to be carefully considered in the next step.

In addition, an image co-correlation algorithm is used to calculate the displacement vector in this work. But it is much less prominent when there are no any apparent structures, such as sunspots or pores inside the field-of-view of the slit-jaw observed in the TiO image channel. There are two solutions for this case. On one hand, we expect the seeing is so good that granular structures can be used to do the image co-correction. On the other hand, we can employ the He 10830 or Hα image channels as the slit-jaw recorder since it is possible that more "apparent structures" can be present in the chromosphere than in the photosphere.

From this work we also realize the necessity of the image stabilizer in order to reduce the image random motion (or shaking) during the scanning, which is quite large compared with the spatial sampling. Otherwise, an enormous amount of data is needed when one wants to achieve high spatial resolution of the 2D spectroscopy by using the technique under study. In addition, given the present parameter settings (i.e., the spatial sampling is 0.45″; five frames are acquired at each slit position, exposure time of the Hα line is about 60 ms), it takes about 60 s to generate a 2D map with the size of 60″ in the scanning direction to achieve a spatial resolution of about 2″. Therefore we think it is not very practical for the high temporal resolution requirement of an active region. A typical size of an active region is about 120″–180″, as a result, about 2–3 minutes are needed to accomplish the scanning.

Acknowledgements We appreciate all the help from colleagues in the NVST team. This work is supported by the National Natural Science Foundation of China (Grant Nos. 11773072, 11573012 and 11473064).

References

Ballesteros, E., Collados, M., Bonet, J. A., et al. 1996, A&AS, 115, 353
Bonaccini, D., & Stauffer, F. 1990, A&A, 229, 272
Cai, Y., Xu, Z., Li, Z., et al. 2017, Sol. Phys., 292, 150
Cao, W., Gorceix, N., Coulter, R., et al. 2010, Astronomische Nachrichten, 331, 636
Collados, M., Rodriguez Hidalgo, I., Ballesteros, E., et al. 1996, A&AS, 115, 367
Fang, C., & Huang, Y. 1995, Progress in Astronomy, 13, 3
Fu, Y., Yuan, S., Xu, F.-y., & Li, Z.-g. 2016, Chinese Patent, ZL2016201053208

Johanneson, A., Bida, T., Lites, B., & Scharmer, G. B. 1992, A&A, 258, 572
Keller, C. U., Stenflo, J. O., Solanki, S. K., Tarbell, T. D., & Title, A. M. 1990, A&A, 236, 250
Liu, Z., Xu, J., Gu, B.-Z., et al. 2014, RAA (Research in Astronomy and Astrophysics), 14, 705
Mein, P. 1977, Sol. Phys., 54, 45
Mein, P., Mein, N., & Bommier, V. 2009, A&A, 507, 531
Mikurda, K., Tritschler, A., & Schmidt, W. 2006, A&A, 454, 359
Puschmann, K. G., Balthasar, H., Beck, C., et al. 2012, in Proc. SPIE, 8446, Ground-based and Airborne Instrumentation for Astronomy IV, 844679
Rimmele, T., & Marino, J. 2006, ApJ, 646, 593
Sütterlin, P., & Wiehr, E. 2000, Sol. Phys., 194, 35
Wang, R., Xu, Z., Jin, Z.-Y., et al. 2013, RAA (Research in Astronomy and Astrophysics), 13, 1240
Xiang, Y.-Y., Liu, Z., & Jin, Z.-Y. 2016, New Astron., 49, 8
Xu, Z., Jin, Z. Y., Xu, F. Y., & Liu, Z. 2014, in IAU Symposium, 300, Nature of Prominences and Their Role in Space Weather, eds. B. Schmieder, J.-M. Malherbe, & S. T. Wu, 117
Xu, Z., Lagg, A., & Solanki, S. K. 2010, A&A, 520, A77
Yang, C.-C., Li, Z.-G., Chen, Y.-C., & Xu, J. 2016, Astronomical Research and Technology, 13, 257